LAWRENCE
LIVERMORE
NATIONAL
LABORATORY

UCRL-JRNL-235460

A Hybrid Method for Accelerated Simulation of Coulomb Collisions in a Plasma

R. Caflisch, C. Wang, G. Dimarco, B. Cohen, A. Dimits

October 10, 2007

SIAM Journal Multiscale Modeling and Simulation

Disclaimer

A Hybrid Method for Accelerated Simulation of Coulomb Collisions in a Plasma

Russel Caflisch and Chiaming Wang *
Giacomo Dimarco †
Bruce Cohen and Andris Dimits ‡

October 9, 2007

Abstract

If the collisional time scale for Coulomb collisions is comparable to the characteristic time scales for a plasma, then simulation of Coulomb collisions may be important for computation of kinetic plasma dynamics. This can be a computational bottleneck because of the large number of simulated particles and collisions (or phase-space resolution requirements in continuum algorithms), as well as the wide range of collision rates over the velocity distribution function. This paper considers Monte Carlo simulation of Coulomb collisions using the binary collision models of Takizuka & Abe and Nanbu. It presents a hybrid method for accelerating the computation of Coulomb collisions. The hybrid method represents the velocity distribution function as a combination of a thermal component (a Maxwellian distribution) and a kinetic component (a set of discrete particles). Collisions between particles from the thermal component preserve the Maxwellian; collisions between particles from the kinetic component are performed using the method of or Nanbu. Collisions between the kinetic and thermal components are performed by sampling a particle from the thermal component and selecting a particle from the kinetic component. Particles are also transferred between the two components according to thermalization and dethermalization probabilities, which are functions of phase space.

*Mathematics Department, University of California at Los Angeles, Los Angeles, CA 90095 USA
†Mathematics Department, University of Ferrara, Ferrara, Italy
‡Lawrence Livermore National Laboratory, Livermore CA 94550 USA

1 Introduction

In many plasma systems, the principal interactions between charged particles are Coulombic. For inter-particle distance d larger than the Debye length λ_D, Coulomb interactions are mediated through electro-magnetic fields governed by a Vlasov equation. On the other hand, if $d < \lambda_D$, these interactions can be described as Coulomb collisions, governed by the Fokker-Planck equation.

The Fokker-Planck equation has a time scale t_{FP}, defined by the rate of change of the particle velocity vector angle. If the characteristic time t_0 of interest is large compared to t_{FP}, then Coulomb interactions will drive the velocity distribution $f(\mathbf{v})$ to its equilibrium, given by a Maxwellian distribution M, with density n_M, velocity $\mathbf{u}_M$ and temperature T_M. Further evolution of the system can be described by continuum equations for n_M, $\mathbf{u}_M$ and T_M. At the other extreme if $t_0 << t_{FP}$, the plasma can be described as collisionless. In the intermediate regime with t_0 and t_{FP} of comparable size, then the kinetics of Coulomb collisions are significant for the evolution of the velocity distribution function for the plasma.

This paper is concerned with Monte Carlo particle methods for simulation of Coulomb collisions in a plasma using binary collisions. One of the earliest and most influential Monte Carlo binary collision models was proposed by T. Takizuka & H. Abe (TA) in 1977 [3] and modified by Nanbu in 1997 [4]. In subsequent work, Bobylev and Nanbu [6] derived a general time-explicit formulation for the approximation of the Fokker-Planck equation by a binary collision model. Wang et al. [9] performed a numerical convergence study for the methods of TA and Nanbu.

The two methods proposed by TA [3] and Nanbu [4] have been widely used in the plasma physics community. Simulation of Coulomb collisions can be a computational bottleneck, however, since the collision times are often very disparate from the characteristic times of interest. This difficulty is compounded by the wide range of collision rates for many problems. For example, consider a velocity distribution in the form of a bump-on-tail; i.e., a near-equilibrium distribution at low velocity with an isolated spike far out on its tail (the "bump"). The rate of collisions between two particles of velocity $\mathbf{v}_1$ and $\mathbf{v}_2$ is proportional to u^{-3} for $u = |\mathbf{v}_1 - \mathbf{v}_2|$. The average rate of collisions between the particles in the central distribution $f \approx M$ is of size $T_M^{-3/2}$ in which T_M is the temperature of the Maxwellian distribution M. The bump may be concentrated at a velocity difference u_B from the center of M with $u_B >> T_M^{1/2}$, so that its rate of interaction with M is

of size $u_B^{-3} << T_M^{-3/2}$. Direct simulation of the Coulomb collisions for a bump-on-tail distribution is dominated by collisions between M and itself, which preserve M but do not affect the evolution of f, and the important interactions of the bump with M will be rare events. This shows that direct simulation of this problem is highly inefficient.

The purpose of this paper is to present a hybrid method for accelerating the simulation of Coulomb collisions. It represents the distribution function as a combination of a thermal component m (a Maxwellian distribution) and kinetic component k (numerically represented as a set of particles). Evolution of the thermal component m is performed using continuum methods based on conservation principles; while evolution of the kinetic component k is performed by Monte Carlo simulation of binary collisions using the method of TA or Nanbu. An interaction between m and k is performed by sampling a particle from m and selecting a particle from k, then treating the interaction as a particle collision. In addition, thermalization (particles moved from k to m) and dethermalization (particles moved from m to k) are performed with probabilities p_T and p_D respectively.

This hybrid method is motivated by a similar hybrid method for rarefied gas dynamics (RGD) developed by Pareschi & Caflisch [5]. In the RGD application, the division between Maxwellian and particle components is performed solely in physical space x; e.g., the probabilities p_T and p_D are functions only of x. For Coulomb collisions, however, the division between the two components must be performed in phase space $(x, \mathbf{v})$, and p_T and p_D are functions of x and $\mathbf{v}$.

The remainder of this paper is organized as follows: The Monte Carlo binary collision methods of TA [3] and Nanbu [4], as well as the general formulation of Bobylev and Nanbu [6], are presented in Section 2, and the hybrid method is formulated in Section 3. Determination of p_T and p_D is performed in Section 4 through a detailed balance requirement and the use of Nanbu's s parameter. Computational results are presented in Section 5, following by conclusions in Section 6.

2 Monte Carlo Simulation of Coulomb Collisions

We first introduce the governing equation for the physical process, and describe the TA and Nanbu Monte Carlo binary collision models for a spatially homogeneous plasma. We consider collisions between N particles consisting of $N/2$ particles from each of two species α and β.

2.1 Governing equation

Coulomb collisions in a plasma can be treated as the simulation of many continuous small-angle binary collisions [2]. The time evolution of the particle distribution in a spatially homogeneous, non-equilibrium plasma is described by the Fokker-Planck equation:

$$\frac{\partial f_\alpha}{\partial t} = (\frac{\delta f_\alpha}{\delta t})_c \tag{1}$$

in which f_α is the distribution function of the α species and $(\frac{\delta f}{\delta t})_c$ is the collision operator defined as (MKS units)

$$(\frac{\delta f_\alpha}{\delta t})_c = -\sum_\beta \frac{\partial}{\partial v_j} \frac{e_\alpha^2 e_\beta^2 \log\Lambda}{8\pi\epsilon_0^2 m_\alpha} \int dv' [\frac{\delta_{jk}}{u} - \frac{u_j u_k}{u^3}][\frac{f_\alpha}{m_\beta}\frac{\partial f_\beta'}{\partial v_k'} - \frac{f_\beta'}{m_\alpha}\frac{\partial f_\alpha}{\partial v_k}]. \tag{2}$$

in which we use the notation $\mathbf{u} = \mathbf{v}_\alpha - \mathbf{v}_\beta$, $u = |\mathbf{u}|$ and $f_\beta' = f_\beta(\mathbf{v}')$. The equation for f_β is similar.

Bobylev and Nanbu [6] derived a general formulation for a binary collision model that approximates the solution of (1) over a time step Δt. The resulting equation (see [6] for further details and definitions) is

$$f_\alpha(\mathbf{v}, t+\Delta t) = \sum_{\beta=1}^{n} \pi_{\alpha\beta} \int_{R^3\times S^2} d\mathbf{v}_\beta d\mathbf{n} D_{\alpha\beta}(\frac{\mathbf{g}\cdot\mathbf{n}}{g}, A_{\alpha\beta}\frac{\Delta t}{g^3}) f_\alpha(\mathbf{v}_\alpha', t) f_\beta(\mathbf{v}_\beta', t). \tag{3}$$

They also found a set of conditions on the kernel $D_{\alpha\beta}$ which ensure that f is an approximate solution of (1), with error of size $O(\Delta t)$. As described in the following, the TA and Nanbu collision models each correspond to Monte Carlo simulation of the integral (3) for a specific choice of $D_{\alpha\beta}$.

2.2 The Collision Model of Takizuka and Abe

Although the TA model was not analyzed in [6], we show that the collision model of TA corresponds to the following formula for D:

$$D_{TA}(\mu, \tau) = (2\pi)^{-1}(2\pi\tau)^{-1/2} e^{-\zeta^2/2\tau} (d\zeta/d\mu) \tag{4}$$

in which

$$\tau = <\zeta^2> = (\frac{e_\alpha^2 e_\beta^2 n_L \log\Lambda}{8\pi\epsilon_0^2 m_{\alpha\beta}^2 u^3})\Delta t \tag{5}$$

and the scattering angle θ in the frame of the relative velocity is defined by

$$\begin{aligned} \theta &= 2\arctan\zeta \\ \mu &= \cos\theta. \end{aligned} \tag{6}$$

Also e_α and e_β are electric charges for the species α and β, n_L is the smaller density of the particle species α and β, Λ is the Coulomb logarithm, $u = |\mathbf{v}_\alpha - \mathbf{v}_\beta|$ is the relative speed, Δt is the time step , and $m_{\alpha\beta} = m_\alpha m_\beta/(m_\alpha + m_\beta)$ is the reduced mass. With the choice $D = D_{TA}$, the convergence criteria of Bobylev and Nanbu in [6] is satisfied, as shown in Appendix A.

A Monte Carlo algorithm for simulation of the integral (3) with the kernel (4) over a single time interval Δt consists of performing the following steps $N/2$ times:

1. Randomly select two particles with velocity $\mathbf{v}_\alpha$ and $\mathbf{v}_\beta$ from the distributions f_α and f_β. This is done by exclusive sampling, so that no particle is selected more than once. This corresponds to the term $f_\alpha f_\beta$ in (3).

2. Sample a value of $\mu = \cos(2\arctan\zeta)$, in which ζ is a Gaussian random variable with mean 0 and variance $\tau =< \zeta^2 >$ and τ is defined by (5) using $u = |\mathbf{v}_\alpha - \mathbf{v}_\beta|$. Define θ by $\theta = 2\arctan\zeta$. This corresponds to the factor $(2\pi\tau)^{-1/2} e^{-\zeta^2/2\tau}(d\zeta/d\mu)$ in D_{TA}.

3. Choose the azimuthal angle ϕ randomly and uniformly from the interval $[0, 2\pi]$. This corresponds to the remaining factor $(2\pi)^{-1}$ in D_{TA}.

4. The new velocities are $\mathbf{v}'_\alpha$ and $\mathbf{v}'_\beta$ defined by

$$\begin{aligned} \mathbf{v}'_\alpha &= \mathbf{v}_\alpha + \frac{m_{\alpha\beta}}{m_\alpha}\Delta\mathbf{u} \\ \mathbf{v}'_\beta &= \mathbf{v}_\beta - \frac{m_{\alpha\beta}}{m_\beta}\Delta\mathbf{u} \end{aligned} \tag{7}$$

in which

$$\begin{aligned} \Delta u_x &= (u_x/u_\perp)u_z\sin\theta\cos\phi - (u_y/u_\perp)u\sin\theta\sin\phi - u_x(1-\cos\theta) \\ \Delta u_y &= (u_y/u_\perp)u_z\sin\theta\cos\phi + (u_x/u_\perp)u\sin\theta\sin\phi - u_y(1-\cos\theta) \\ \Delta u_z &= -u_\perp\sin\theta\cos\phi - u_z(1-\cos\theta) \\ \mathbf{u} &= \mathbf{v}_\alpha - \mathbf{v}_\beta. \\ u_\perp &= \sqrt{u_x^2 + u_y^2}. \end{aligned} \tag{8}$$

5. Replace the velocities $\mathbf{v}_\alpha$ and $\mathbf{v}_\beta$ by $\mathbf{v}'_\alpha$ and $\mathbf{v}'_\beta$. This corresponds to the appearance of $\mathbf{v}'_\alpha$ and $\mathbf{v}'_\beta$ as the arguments of f_α and f_β in (3).

These are exactly the steps of the algorithm described in the work of TA [3]. Note that in this algorithm, as well as in the algorithm of Nanbu and the general formulation of [6], every particle collides exactly once in each time interval.

2.3 Nanbu's Collision Model

As described in [6], the collision model of Nanbu corresponds to the following formula for D:

$$D_{Nanbu}(\mu, \tau) = \frac{A}{4\pi \sinh A} \exp \mu A. \tag{9}$$

Monte Carlo simulation using this kernel over a single time interval Δt consists of performing the following steps $N/2$ times:

1. Randomly select two particles with velocity $\mathbf{v}_\alpha$ and $\mathbf{v}_\beta$ from the distribution f. This is done by exclusive sampling, so that no particle is selected more than once.

2. Calculate the quantities s and A solving

$$s = 2\tau \tag{10}$$

$$\coth A - A^{-1} = e^{-s} \tag{11}$$

   with τ defined by (5), using $u = |\mathbf{v}_\alpha - \mathbf{v}_\beta|$ in the definition (5) of τ.

3. Sample a value of the random variable μ from the interval $[-1, 1]$ with probability density

$$f(\mu) = 2\pi D_{Nanbu} = A(2 \sinh A)^{-1} e^{A\mu} \tag{12}$$

   and define θ by $\mu = \cos(\theta)$.

4. Choose the azimuthal angle ϕ randomly and uniformly from the interval $[0, 2\pi]$.

5. The new velocities are $\mathbf{v}'_\alpha$ and $\mathbf{v}'_\beta$ are defined as in (7) and (8).

6. Replace the velocities $\mathbf{v}_\alpha$ and $\mathbf{v}_\beta$ by $\mathbf{v}'_\alpha$ and $\mathbf{v}'_\beta$.

These are exactly the steps of the algorithm described in the work of Nanbu [3], with some minor changes in notation, for consistency with the TA method.

In the remainder of the paper, the collisions are assumed to be between particles from a single species so that the subscripts α and β are dropped. In addition, the distribution function will be assumed to be spatially homogeneous, so that particle position can be neglected.

3 The Hybrid Method

The hybrid method is based on representation of the velocity distribution function f as a combination of a thermal component m and a kinetic component k; i.e.,

$$f(\mathbf{v}) = m(\mathbf{v}) + k(\mathbf{v}). \tag{13}$$

The thermal component is a Maxwellian distribution

$$m(\mathbf{v}) = n_m(2\pi T_m)^{-3/2} \exp\left(-|\mathbf{v} - \mathbf{u}_m|^2/2T_m\right). \tag{14}$$

Because of the (expected) slow interaction of the thermal component m with the kinetic component k, the average density, velocity and temperature n_m, $\mathbf{u}_m$ and T_m of m are not assumed to be those of the full distribution f. This explains the difference between the notation m and M, since M is assumed to density, velocity and temperature that are equal to those of f.

Denote n_m and n_k to be the effective number of particles in the thermal and kinetic components, respectively, of f. At present these numbers will be kept to be even integers. The kinetic component will be simulated using a set of discrete particles; i.e.,

$$g(\mathbf{v}) = \sum_{i=1}^{n_k} \delta(\mathbf{v} - \mathbf{v}_i). \tag{15}$$

In each time interval, the simulation steps are the following:

1. Determine the number of collisions of each type; i.e.,

   - $n_{mm} = n_m^2/2(n_k + n_m)$ is the number of collisions between 2 m particles.
   - $n_{kk} = n_k^2/2(n_k + n_m)$ is the number of collisions between 2 k particles.

- $n_{mk} = n_m n_k/(n_k + n_m)$ is the number of collisions between an m particle and a k particle.

2. Perform the collisions.

   - The $m - m$ collisions do not change the distribution m, so they do not need to be performed.
   - For each $k - k$ collision, select two particles $\mathbf{v}_1$ and $\mathbf{v}_2$ from k. Perform a collision between them, as in the method of TA or Nanbu, to get new velocities $\mathbf{v}_1'$ and $\mathbf{v}_2'$. In k, replace $\mathbf{v}_1$ and $\mathbf{v}_2$ by $\mathbf{v}_1'$ and $\mathbf{v}_2'$.
   - For each $m - k$ collisions, sample a particle $\mathbf{v}_m$ from m and select a particle $\mathbf{v}_k$ from k. Perform a collision between them, as in the method of TA or Nanbu, to get new velocities $\mathbf{v}_m'$ and $\mathbf{v}_k'$. The postcollision velocity $\mathbf{v}_k'$ replaces $\mathbf{v}_k$ in k.

3. Apply thermalization and dethermalization.

   - For each post-collision particle $\mathbf{v}'$ (i.e., $\mathbf{v}_1'$, $\mathbf{v}_2'$ or $\mathbf{v}_k'$ from the previous step), thermalize $\mathbf{v}'$ with probability $p_T(\mathbf{v}')$. This is done by removing $\mathbf{v}'$ from k (in the next step its number, momentum and energy will be added to m).
   - For each post-collision particle $\mathbf{v}_m'$, dethermalize $\mathbf{v}_m'$ with probability $p_D(\mathbf{v}_m')$. This is done by adding $\mathbf{v}_m'$ to k (in the next step its number, momentum and energy will be subtracted from m).

4. Apply conservation.

   - Adjust the number n_k of particles in k, due to thermalization and dethermalization.
   - Adjust the number, momentum and energy of m, due to thermalization and dethermalization. This is most easily performed by requiring that the total number, momentum and energy of $f = m + k$ be the same before and after the collisions.

A possible problem with this algorithm is that sampling velocities $\mathbf{v}_m$ from m may remove too much energy from m. This can be avoided by conservative sampling. First sample all n_{mk} velocities from m and then shift and scale these so that the average momentum and energy of the sampled particles is the same as the average momentum and energy of m.

4 Choice of p_D and p_T

4.1 Detailed Balance Condition

Consider an equilibrium distribution M represented as

$$M = m + k = f \tag{16}$$

in which m is the continuum component and k is the kinetic component. Note that m is an equilibrium, but m is not necessarily equal to M. In Appendix B, detailed balance is used to derive conditions on p_D and p_T, starting from the scattering integral of (3) with the inclusion of thermalization/dethermalization. Although this is the theoretically correct approach, it does not lead to explicit conditions on p_D and p_T.

In this section, we adopt a simpler approach by requiring that thermalization/dethermalization applied to all of $f = m+k$ does not change m and k, if $f = M$ is a Maxwellian. This is performed as follows: Apply thermalization to k with probability p_T and dethermalization to m with probability p_D. Also define a projection Π_M onto equilibria, i.e., $\Pi_M f$ is the Maxwellian with same $(\rho, \mathbf{u}, T)$ as f. The resulting distribution is

$$f' = \Pi_M((1-p_D)m + p_T k) + p_D m + (1-p_T)k. \tag{17}$$

Now assume that $f = m+k = M$ and require that the form of f is conserved; i.e.,

$$\begin{aligned} m &= \Pi_M((1-p_D)m + p_T k) \\ k &= p_D m + (1-p_T)k. \end{aligned} \tag{18}$$

It follows that

$$k = (p_D/p_T)m \tag{19}$$

$$M = (1 + p_D/p_T)m. \tag{20}$$

Denote

$$\gamma = M/m. \tag{21}$$

For simplicity assume that

$$\mathbf{u}_M = \mathbf{u}_m = 0 \tag{22}$$

or more generally that $\mathbf{u}_M = \mathbf{u}_m$. This is not generally true, but is a reasonable assumption if $f = M$. Then look for

$$\gamma(\mathbf{v}) = ce^{|\mathbf{v}|^2/2\tau} \tag{23}$$

in which

$$\begin{aligned} c &= (n_M/n_m)(T_m/T_M)^{3/2} && (24)\\ \tau^{-1} &= T_m^{-1} - T_M^{-1}. && (25) \end{aligned}$$

Note that $m < M$ for all $\mathbf{v}$, so that

$$T_m < T_M. \tag{26}$$

Insertion of (25) into (19), shows that the detailed balance requirement for p_D and p_T is

$$1 + p_D/p_T = ce^{|\mathbf{v}|^2/2\tau}. \tag{27}$$

4.2 Velocity-based choice of p_D and p_T

Look for p_T, p_D to satisfy

$$\begin{aligned} p_T &= 1 \qquad \text{for } |\mathbf{v}| < v_1 \\ p_D &= 1 \qquad \text{for } |\mathbf{v}| > v_2. \end{aligned} \tag{28}$$

in which v_1 and v_2 are constants with $v_1 < v_2$. Define

$$\begin{aligned} p_D &= \sqrt{\alpha(\gamma - 1)} \\ p_T &= \sqrt{\alpha/(\gamma - 1)} \end{aligned} \tag{29}$$

which automatically satisfies (27). For a given choice of v_1, v_2, set

$$\begin{aligned} c &= 1 \\ \tau &= (4\log 2)^{-1}(v_1^2 + v_2^2) \\ \gamma_1 &= \gamma(v_1) = e^{v_1^2/2\tau} \\ \gamma_2 &= \gamma(v_2) = e^{v_2^2/2\tau} \\ \alpha_1 &= \alpha(v_1) = (\gamma_1 - 1) \\ \alpha_2 &= \alpha(v_2) = (\gamma_2 - 1)^{-1}. \end{aligned} \tag{30}$$

The choice of τ was made so that

$$0 < \alpha_1 < 1, \quad 0 < \alpha_2 < 1 \tag{31}$$

i.e.

$$v_1^2/2\tau < \log 2 < v_2^2/2\tau. \tag{32}$$

Since $p_D(v_1) = \alpha_1$ and $p_T(v_2) = \alpha_2$, the construction below will ensure that $0 \le p_D \le 1$ and $0 \le p_T \le 1$.

Equations (28) and (29) determine α for $|\mathbf{v}| < v_1$ (i.e., for $\gamma < \gamma_1$) and $|\mathbf{v}| > v_2$ (i.e., for $\gamma > \gamma_2$). Define α in the interval $\gamma_1 < \gamma < \gamma_2$ by interpolation with respect to γ to get

$$\alpha = \begin{cases} (\gamma - 1) & \text{for } |\mathbf{v}| < v_1 \\ \alpha_1 + \frac{(\gamma - \gamma_1)}{\gamma_2 - \gamma_1}(\alpha_2 - \alpha_1) & \text{for } v_1 < |\mathbf{v}| < v_2 \\ (\gamma - 1)^{-1} & \text{for } v_2 < |\mathbf{v}|. \end{cases} \tag{33}$$

Figure 1 shows a typical graph of the probabilities p_T and p_D as functions of v.

Note that the choice $c = 1$, along with (24) determines the mass of the Maxwellian component of m to be

$$n_m = n_M (T_m/T_M)^{3/2}. \tag{34}$$

In addition, the values of p_T for $|\mathbf{v}| < v_1$ and p_D for $v_2 < |\mathbf{v}|$ could be set to values $\bar{p}_T$ and $\bar{p}_D$ that are different than 1 and the formulas above could be modified to accommodate this change.

4.3 s-Based Method

In order to correctly incorporate the time step Δt into the hybrid method, we base the thermalization/dethermalization probabilities p_T and p_D on Nanbu's parameter s rather than $\mathbf{v}$. Choose values of s_1 and s_2 with $s_1 > s_2 > 0$. For each value of Δt, determine values of v_1 and v_2 so that $s(v_1, \Delta t) = s_1$ and $s(v_2, \Delta t) = s_2$. Then use the method in Section 4.2 with these values of v_1 and v_2.

The choice of p_T and p_D described above is somewhat arbitrary; optimizing this choice subject to the condition (27) (or some improvement on this condition, as in Appendix B) could lead to an improved hybrid method.

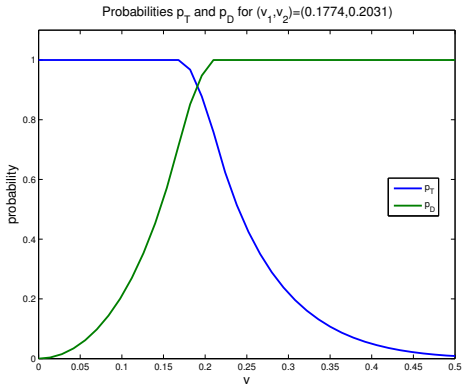

Figure 1: Probabilities p_T and p_D for thermalization and dethermalization as functions of $v = |\mathbf{v}|$, in which $v_1 = 0.1774$ and $v_2 = 0.2031$.

5 Computational Results

5.1 Bump-on-Tail and Maxwellian Initial Data

As a test of the hybrid method, we performed a series of computations for initial data that is a bump-on-tail. As discussed in Section 1, this problem involves two widely separated time scales for Coulomb interactions, so that it is well suited for the hybrid method: a fast time scale for collisions between particles within the central Maxwellian and a slower time scale for those between particles from the central Maxwellian and the bump. We also performed computation for initial data that is Maxwellian, in order to test the consistency of the hybrid method.

The bump-on-tail initial distribution $f_0(\mathbf{v})$ is specified to be a combination of a Maxwellian $M_0(\mathbf{v})$ and a bump $g_0(\mathbf{v})$. The bump is specified to be approximately a δ-function containing 10% of the mass of the distribution and centered at $\mathbf{v} = (v_b, 0, 0)$ with $v_b = a\sqrt{T_e/m_e}$. The Maxwellian M_0 is centered and scaled so that the average velocity is 0 and the temperature is T_e. The examples presented here are for two different choices of a: $a = 4$ in problem BOT4 and $a = 3$ in problem BOT3.

The computation is performed in a dimensionless formulation in which the electron mass is $m_e = 1$, and the electron density n_e and temperature T_e were chosen to be $n_e = 0.1$ and $T_e = 0.05065776$. For a characteristic

time for the collision process, we use

$$\begin{aligned} t_c &= u_{th}^3 \left(\frac{q_e^2}{\epsilon_0 m_e/2} \right)^{-2} \left(\frac{n_e \log \Lambda_e/2}{4\pi} \right)^{-2} \\ u_{th} &= \sqrt{6T_e/m_e} \end{aligned} \tag{35}$$

which has value $t_c = 5.348275$. Unless otherwise state, the number of particles is $N = 128,000$.

Note that in all the simulation examples reported here, the plasma is spatially homogeneous so that there are no electromagnetic fields and no convection.

5.2 Consistency Tests

As a consistency test, we first performed computations for Maxwellian initial data $M(\mathbf{v})$, with density $n_e = 0.1$, temperature $T_e = 0.05065776$ and zero average velocity, as stated above.

Figure 2 shows the result of simulation using the hybrid method with this initial data for two different values of the hybrid parameters s_1 and s_2. The hybrid method parameters are $(s_1, s_2) = (2, 1)$ on the left and $(s_1, s_2) = (1, 0.5)$ on the right; the time step is $\Delta t = t_c/100$. The total distribution $f = m + k$ (upper curves) and the thermal component m (lower curves) of the distribution are shown as a function of the x-velocity v_x at three times $t = 0$, $t = 8.8t_c$, $t = 18.5t_c$. The initial data consists of all particles; i.e., $k = M$ and $m = 0$ for $t = 0$. The total distribution f is the same for all t, which is consistent with its Maxwellian initial data. Although it starts at 0, by time $t = 8.8t_c$ (i.e. after an initial transient), the thermal component m has reached a nonzero steady state which is the same as its value at $t = 18.5t_c$. This demonstrates the success of the detailed balance condition (27). Also shown is the thermal component $m_{theoretical}$ predicted from the choice $c = 1$ for which the density is given by (24). Although the theoretical prediction is correct for the hybrid simulation on the left, it is incorrect for the simulation on the right. A better theory (better than that of Section 4.1) could help to improve the formulation of the hybrid method.

Next we perform a comparison of the s-based and v-based hybrid methods on the bump-on-tail problem BOT4. Set $(s_1, s_2) = (3, 2)$ and $\Delta t = t_c/10$. The corresponding values of v_1 and v_2, satisfying $s = 2\tau$ from (10) with $\tau = \tau(v, \Delta t)$ defined by (5), are $(v_1, v_2) = (0.1774, 0.2031)$. The top row of graphs in Figure 3 shows the results for the v-based method (upper

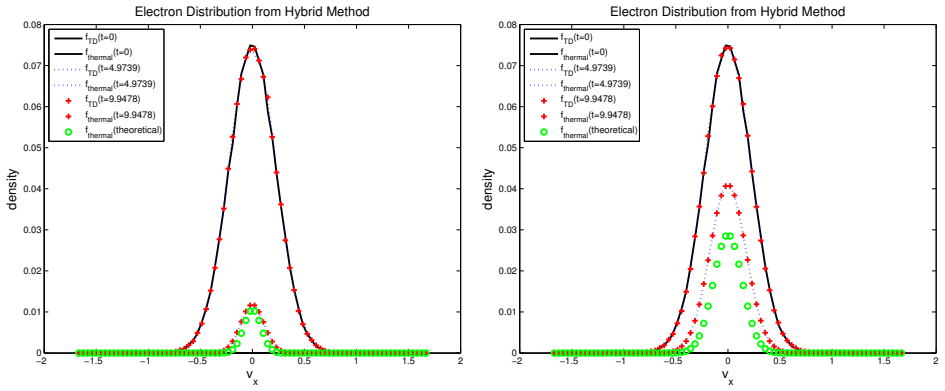

Figure 2: Comparison of the hybrid method for Maxwellian (equilibrium) initial data at three different times ($t = 0$, $t = 8.8t_c$, $t = 18.5t_c$). The plots show the full distribution function $f(v_x)$ (upper curves) and the thermal component $m(v_x)$ (lower curves), as well as the thermal component (circles) predicted from the theory of Section 4.1. The hybrid method parameters are $(s_1, s_2) = (2, 1)$ (left) and $(s_1, s_2) = (1, 0.5)$ (right).

left) and the s-based method (upper right) with these parameters. Each graph shows a comparison of results from the hybrid (blue dashed line) and Nanbu (red solid line) methods at time at time $t = 1.3t_c$. These graphs are identical (and show good agreement between the hybrid and Nanbu methods) since the values of (v_1, v_2) were chosen to be in agreement with the values of (s_1, s_2).

Now keep the same values of (v_1, v_2) and (s_1, s_2), but change the time step to $\Delta t = t_c/1000$. The results (on the lower graphs of Figure 3) show that the accuracy of the v-based method (lower left) deteriorates as the time step is decreased; whereas the accuracy of the s-based method (lower right) improves. In addition, the thermal component (green dotted line) for the s-based method decreases with smaller time step, so that the efficiency of the s-based method decreases. This gain in accuracy but loss of efficiency for the s-based method is acceptable dependence on Δt; while the loss of accuracy with decreased Δt for the v-based method is not acceptable.

The reason for this dependence on time step is easily understood. For the v-based method, the probability of thermalization is independent of the time step Δt, so that for small Δt the thermalization is too strong. On the other hand, for the s-based method, the thermalization per time step decreases as

Δt decreases, and the function $s(\Delta t)$ has the correct dependence on Δt, as well as on density and temperature.

5.3 Simulation for the Evolution of a Bump-on-Tail

Figures 4 and 5 show a comparison of the solutions computed by the hybrid (blue dashed line) and Nanbu (red solid line) methods for bump-on-tail problems BOT4 and BOT3, respectively, at various times between the initial time and a final time $T = 7.2t_c$. For the hybrid method the parameters are $(s_1, s_2) = (3, 2)$ and $\Delta t = t_c/10$. The thermal component of the hybrid representation (13) (green dotted line) is also plotted. Both figures show very agreement between the hybrid and Nanbu curves, providing a measure of validation for the hybrid method.

For problem BOT4 in Figure 4 the parameters are $\Delta t = t_c/10$ and $(s_1, s_2) = (3, 2)$. The thermal component of the hybrid representation (13), which contains about 1/3 of the particles.

For problem BOT3 in Figure 5 the parameters are $\Delta t = t_c/100$ and $(s_1, s_2) = (1, 0.5)$. In this problem, the thermal component of the hybrid representation contains about 1/7 of the particles.

5.4 Variation of Parameters Δt, s_1 and s_2

In order to understand the effect of the parameters Δt, s_1 and s_2 on the solution of the hybrid method, we performed computation for the bump-on-tail problem BOT4 of Figure 4 with different parameter values. Figures 6 and 7 show the solution of BOT4 at $t = 1.2t_c$ and $t = 3.6t_c$, respectively. In each figure, the time step is $\Delta t = t_c/10$ for the graphs in the left column and $\Delta t = t_c/100$ for those in the right column. Also, the values of (s_1, s_2) are $(s_1, s_2) = (1, 0.5)$ for the graphs in top row, $(s_1, s_2) = (2, 1)$ for the middle row and $(s_1, s_2) = (3, 2)$ for the bottom row.

In Figure 6 at an early time, the bump is still distinct but is shifted and diffused from its original position and shape. In Figure 7 at a later time, the bump is no longer a distinct peak but has been reduced to a shelf in the distribution function. Comparison of the figures shows that for larger Δt or smaller s_1 and s_2 the bump is overthermalized, with the result that it is shifted too far toward the center and becomes too wide. As Δt is decreased and s_1 and s_2 are increased, the accuracy of the computation dramatically improves. On the other hand, the size of the thermal component, which determines the efficiency of the hybrid method, is larger for larger values of

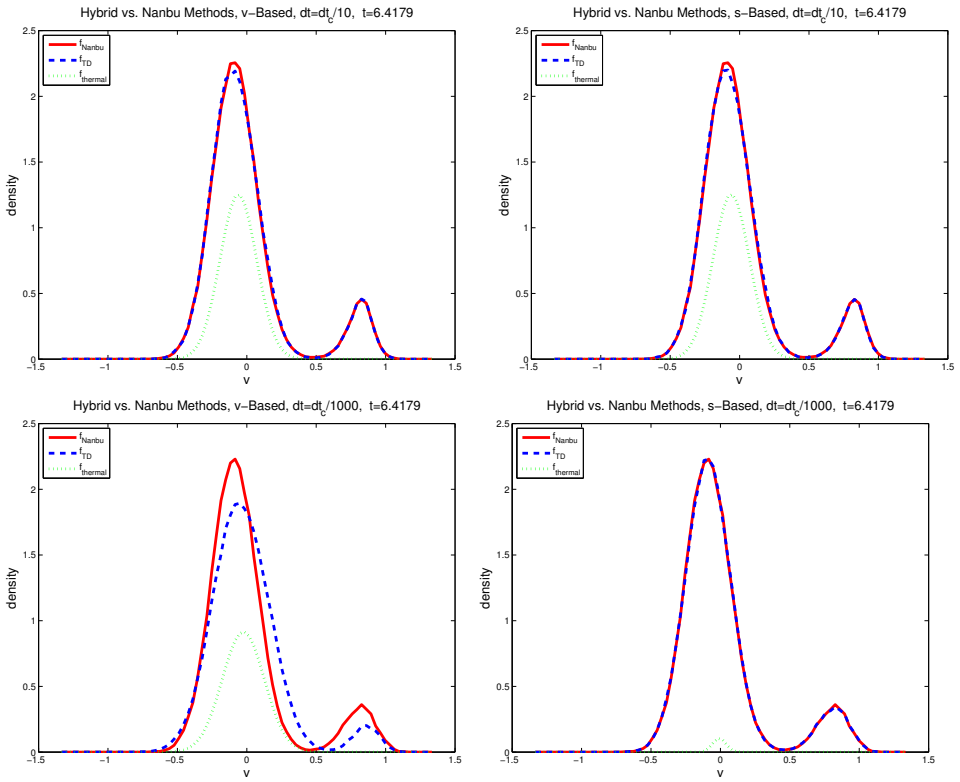

Figure 3: Comparison of the v-based and s-based versions of the hybrid method for different time steps Δt. The plots show the velocity distribution function from the hybrid (blue dashed line) and Nanbu (red solid line) method, as well as the thermal component for the hybrid method (green dotted line), for problem BOT4 at time $t = 1.3t_c$. The time step is $\Delta t = t_c/10$ for the top row and $\Delta t = t_c/1000$ for the bottom row. The left column comes from the v-based method with $(v_1, v_2) = (0.1774, 0.2031)$, while the right column comes from the s-based method with $(s_1, s_2) = (3, 2)$.

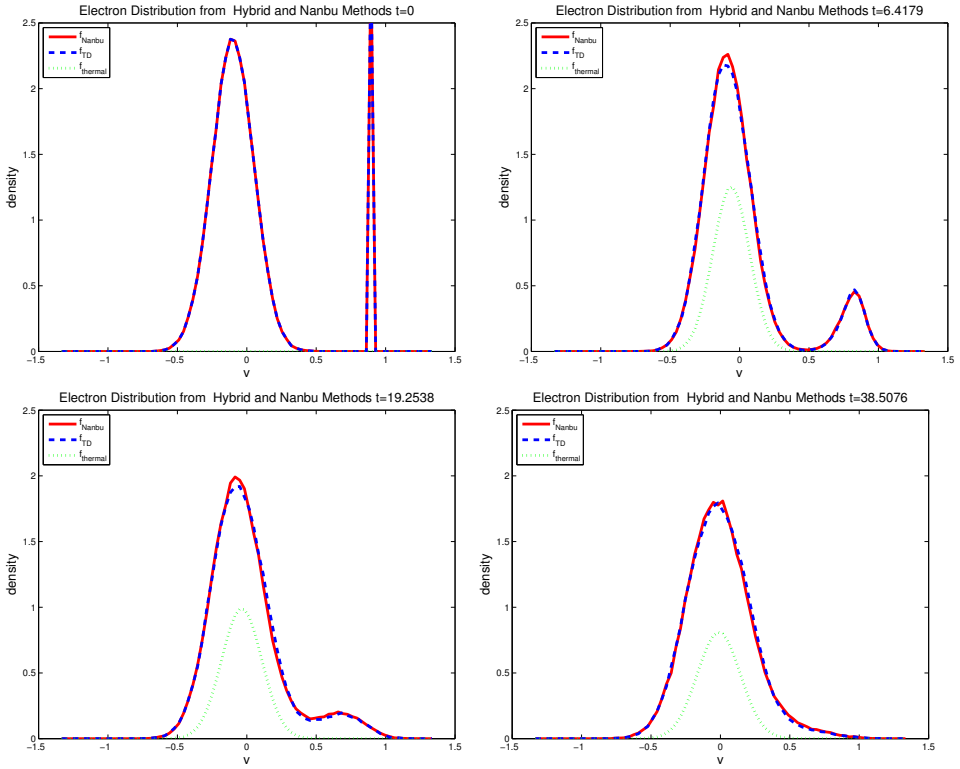

Figure 4: Comparison of the hybrid (blue dashed line) and Nanbu (red solid line) solutions at different times $t = 0$ (upper left), $t = 1.2t_c$ (upper right), $t = 3.6t_c$ (lower left) and $t = 7.2t_c$ (lower right). The computations use $\Delta t = t_c/10$ and $(s_1, s_2) = (3, 2)$ for the problem BOT4.

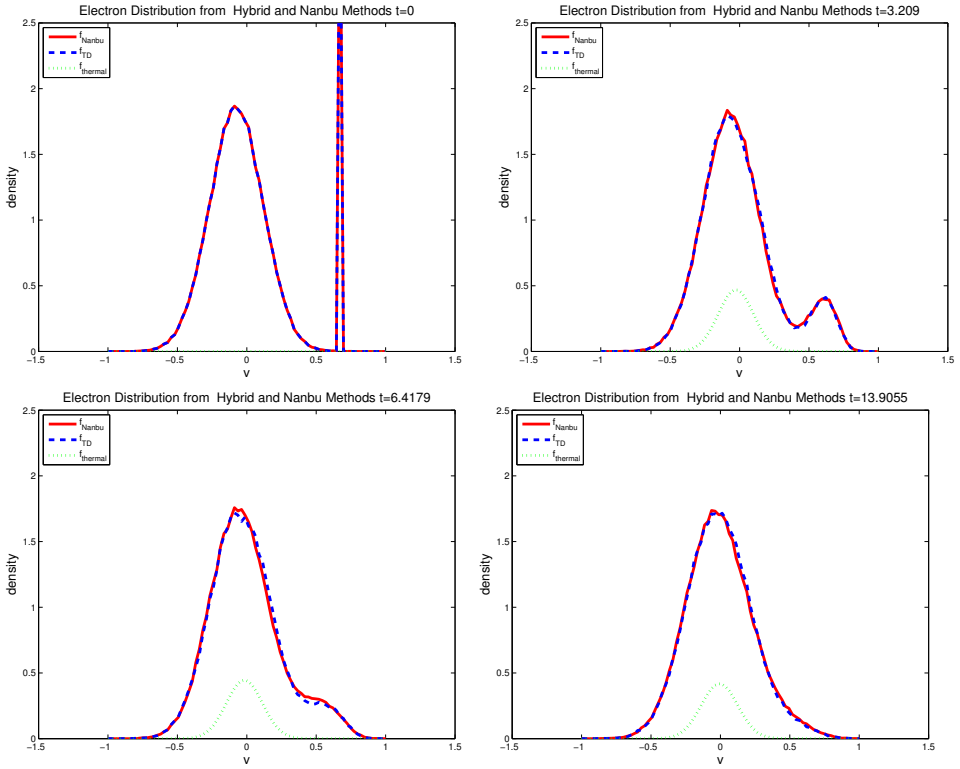

Figure 5: Comparison of the hybrid (blue dashed line) and Nanbu (red solid line) solutions at different times $t = 0$ (upper left), $t = 0.6t_c$ (upper right), $t = 1.2t_c$ (lower left) and $t = 2.6t_c$ (lower right). The computations use $\Delta t = t_c/100$ and $(s_1, s_2) = (1, 0.5)$ for the problem BOT3.

Δt and smaller values of s_1 and s_2. This shows a trade-off between efficiency and accuracy of the hybrid method.

5.5 Accuracy and Efficiency for the Hybrid Method

In order to measure the performance of the hybrid method, we first define quantities γ_{eff} and γ_{acc} that measure the efficiency and accuracy of the computations, as

$$\gamma_{eff} = \frac{1}{Tn_f}\int_0^T n_m dt \tag{36}$$

$$\gamma_{acc} = \frac{1}{Tn_f}\int\int_0^T |f - f_H| dt dv. \tag{37}$$

Efficiency of the method is meant to be the ratio between the computational savings of the hybrid method and the computational cost of the standard method. Since the computational effort is roughly proportional to the number of particles in the simulation, the efficiency measure γ_{eff} is the ratio of n_m and n_f in which n_m and n_f are the number of particles in the Maxwellian component m and the total number of particles in f. As a measure of accuracy, γ_{acc} is the relative size of L^1 norm (in v and t) of the error.

We performed a series of computations for parameters in the range $0.2 \leq s_2 \leq 2$ and $0.2 \leq s_1 - s_2 \leq 2$, and for time step $\Delta t = t_c/10$ and final time $T = 74t_c$. The resulting values of γ_{eff} and γ_{acc} are presented in contour plots in Figure 8, which shows them to be constant along (nearly) linear curves in the (s_1, s_2) plane. A scatter plot of these values of γ_{eff} and γ_{acc} in the graph on the left in Figure 9. This graph shows that these values collapse onto a single curve, so that γ_{acc} is a single-valued function of γ_{eff}. This shows that for any level of accuracy there is a resulting level of efficiency. Further variation of the parameters (s_1, s_2) does not change performance of the method. This conclusion holds only within the context of specific choice of p_D and p_T. The relationship between accuracy and efficiency could be changed by considering a wider class of functions p_D and p_T.

In the graph on the left in Figure 9, the values of accuracy γ_{acc} appear to taper off to a finite nonzero value. The graph on the right in Figure 9 shows that statistical fluctuations due to the finite value N of particles contribute importantly to this residual error. There may be an additional significant contribution to the total error due to finite Δt effects. This graph shows a plot of γ_{acc} versus γ_{eff} for three values of N: $N = 32,000$, $N = 128,000$ and $N = 512,000$. The values of (s_1, s_2) are $4 < s_2 < 6.2$ and $s_1 = s_2 + 2$,

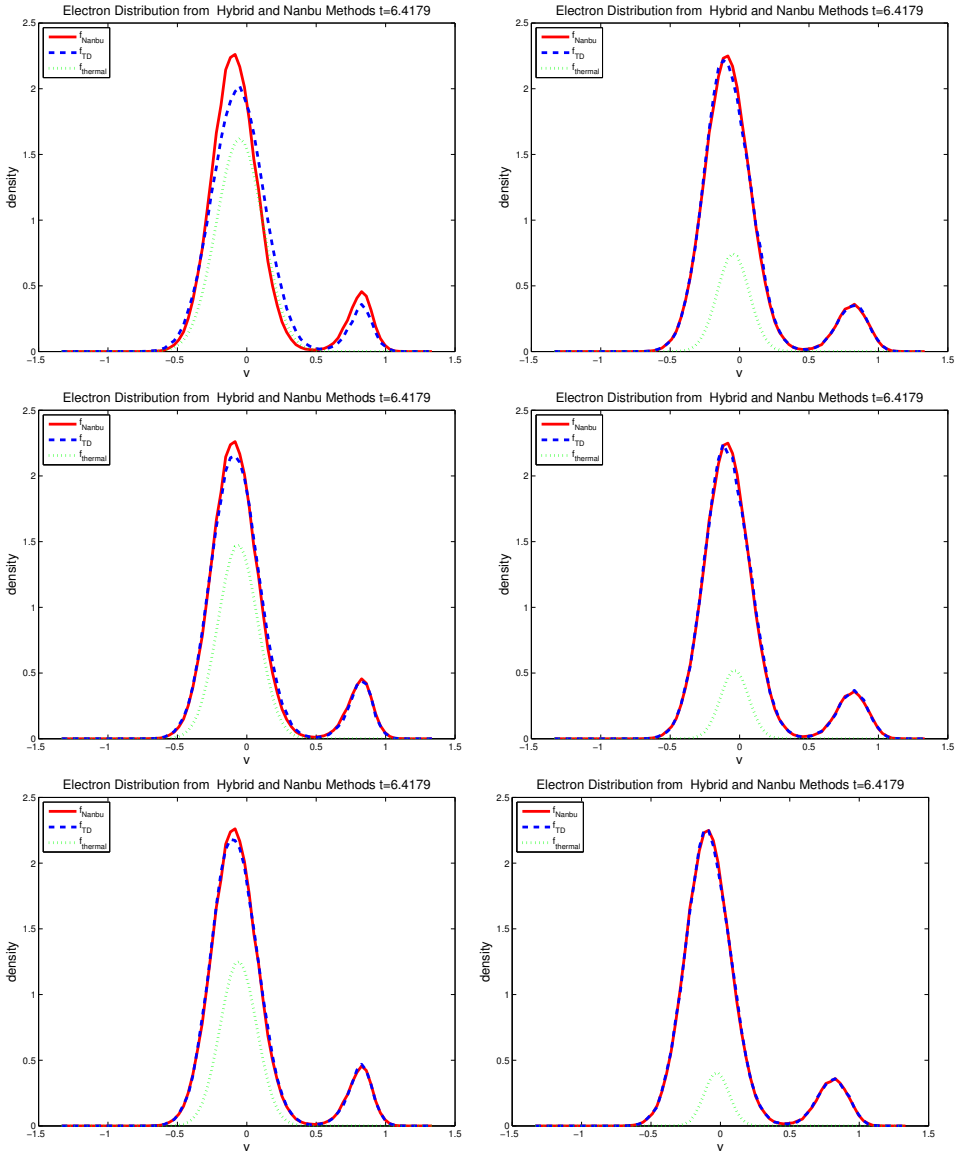

Figure 6: Comparison of the hybrid (blue dashed line) and Nanbu (red solid line) solutions for different values of the parameters Δt, s_1 and s_2. The values of Δt are $t_c/10$ for the left column and $t_c/100$ for the right column. The values of (s_1, s_2) are $(1, 0.5)$ for the top row, $(2, 1)$ for the middle row and $(3, 2)$ for the bottom row. These simulations are for problem BOT4 of Figure 4 at time $t = 1.2t_c$.

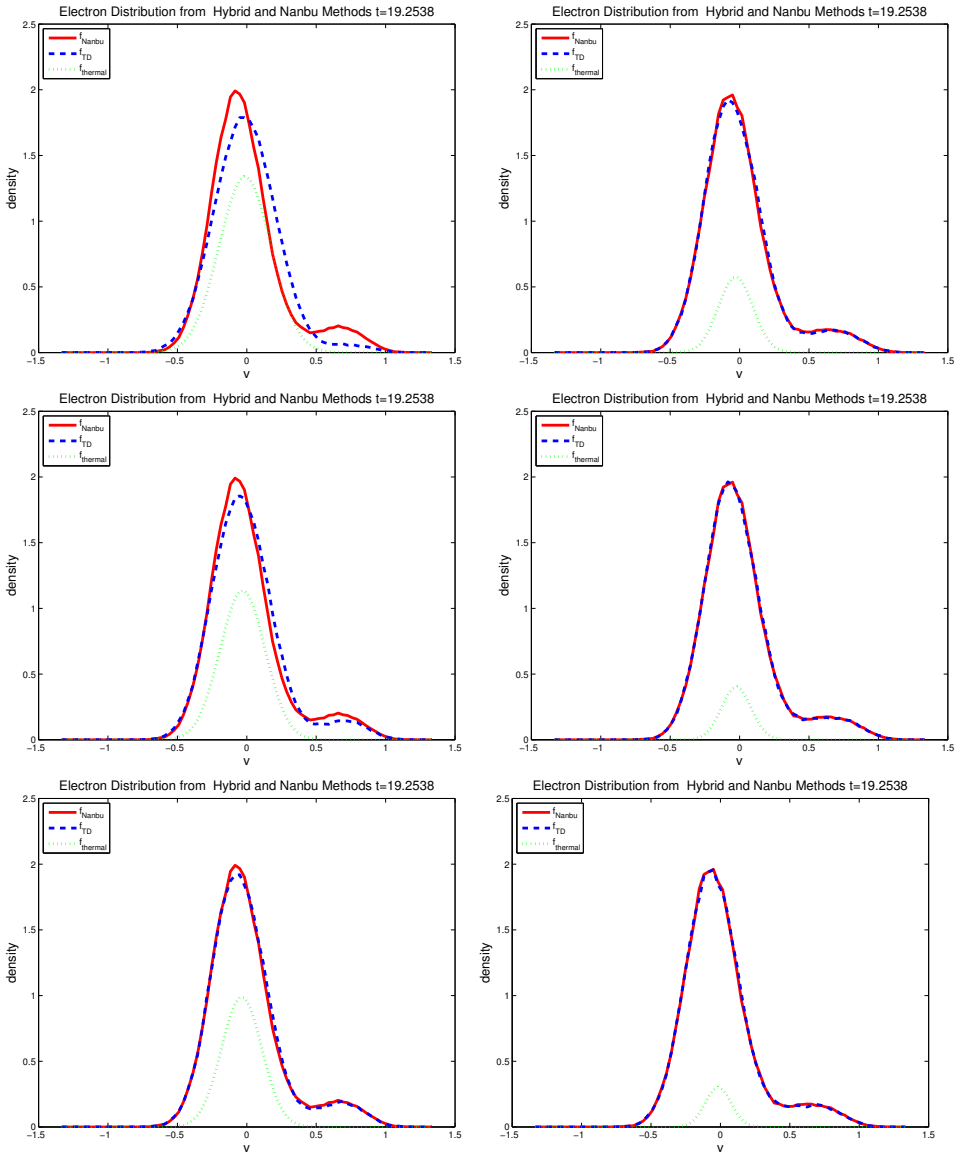

Figure 7: Same as Figure 6 but at later time $t = 3.6t_c$.

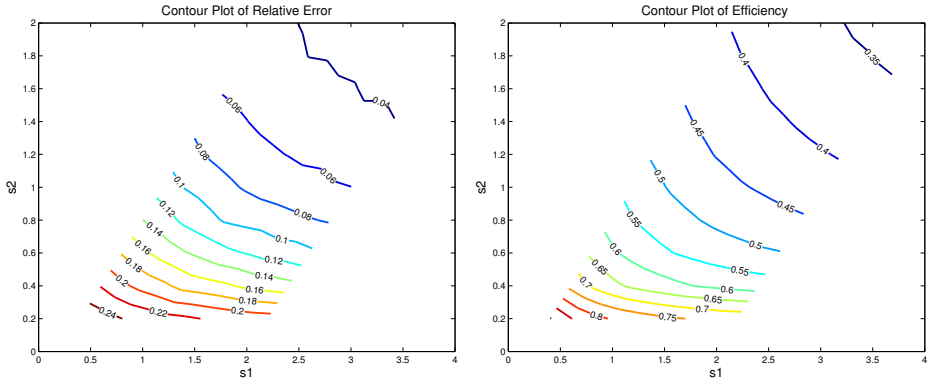

Figure 8: Error (left) and Efficiency (right) for the hybrid method applied to the problem BOT4 of Figure 4, as functions of the parameters s_1 and s_2.

which are larger than those in Figure 8 and the graph on the left of Figure 9.

Comparison of the results for $N = 32,000$, $N = 128,000$ and $N = 512,000$ in this graph shows the errors γ_{acc} are smaller for larger values of N. More specifically, for larger values of N, the linear decrease of γ_{acc} continues for smaller values of γ_{eff}, and the remaining residual value of γ_{acc} is smaller.

6 Conclusions

The hybrid method developed above combines continuum and particle descriptions for the evolution of a velocity distribution function through Coulomb interactions. The method includes particle interactions, but since the examples here are spatially homogeneous, the continuum description is just an equilibrium Maxwelllian distribution.

Because of the variation of the interaction rate as a function of particle velocity, the division of f between particles and continuum must be performed as a function of velocity. In the hybrid method of this paper, the velocity dependence is effected through velocity dependence of the thermalization and dethermalization probabilities $p_T(v)$ and $p_D(v)$.

The specific choice of $p_T(v)$ and $p_D(v)$ is ad hoc and formulated in terms of two parameters s_1 and s_2 (or v_1 and v_2) as well as Δt. The simulations

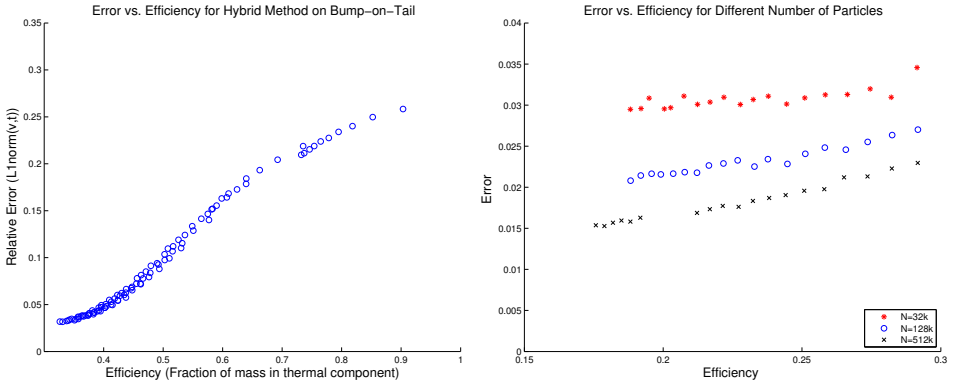

Figure 9: Error vs. efficiency for the bump-on-tail problem of Figure 4. The graph on the left is a scatter plot of the values of error and efficiency from Figure 8. The graph at right shows a continuation of error and efficiency for larger values of s_1 and s_2 and for values of N given by $32,000$ (stars), $128,000$ (circles) and $512,000$ (x's).

show that for this method the efficiency is a single-valued function of the accuracy of the method. Therefore the method provides a certain level of efficiency (acceleration) for prescribed accuracy of the hybrid approximation.

Further development of the hybrid method could include development of alternative formulations and optimization of $p_T(v)$ and $p_D(v)$, modification of the method so that that the distribution is completely thermalized as $t \to \infty$ (i.e., $m \to M$ and $k \to 0$), development of a mathematical foundation for this method, and improved analysis of the detailed balance properties of the method. Applications of the method will be carried out for spatially inhomogeneous problems, especially those having the character of a bump-on-tail.

7 Acknowledgments

This work performed under the auspices of the U.S. Department of Energy by the University of California, Los Angeles, under grant DE-FG02-05ER25710, and by Lawrence Livermore National Laboratory under Contract DE-AC52-07NA27344. The work was supported by the Office of Advanced Scientific Computing Research, DOE Office of Science, under the Multiscale Initiative program.

References

[2] L. Spitzer, Jr., Physics of Fully Ionized Gases, 2nd ed. (Interscience, New York, 1967).

[3] T. Takizuka and H. Abe, J. Comp. Phys. 25 (1977).

[4] K. Nanbu, Phys. Rev. E. 55 (1997).

[5] R. E. Caflisch and L. Pareschi. J. Compt. Phys. 154, 96 (1999).

[6] A. V. Bobylev and K. Nanbu, Physical Review E, Vol 61, No. 4, p. 4576-4582 (2000).

[7] M. N. Rosenbluth, W. M. MacDonald, and D. L. Judd, Phys. Rev. 107, 1 (1957).

[8] B. A. Trubnikov, Review of Plasma Physics (Consultant Bureau, New York, 1965), Vol. 1, p. 105.

[9] C. Wang, T. Lin, R.E. Caflisch, B. Cohen and A. Dimits, "Particle Simulation of Coulomb Collisions: Comparing the methods of Takizuka & Abe and Nanbu" (2006) under review.

A Analysis of the Scattering Kernel D for the Takizuka & Abe Method

The convergence criteria from Bobylev and Nanbu (equations (48a)-(48c) in [6]) are that

$$D(\mu,\tau) \geq 0 \tag{38}$$

$$2\pi \int_{-1}^{1} d\mu D(\mu,\tau) = 1 \tag{39}$$

$$\lim_{\tau\to 0} D(\mu,\tau) = (2\pi)^{-1}\delta(1-\mu) \tag{40}$$

$$\lim_{\tau\to 0}(2\pi/\tau)\int_{-1}^{1} d\mu D(\mu,\tau)[1-P_\ell(\mu)] = \ell(\ell+1) \tag{41}$$

in which P_ℓ is the Legendre polynomial for positive integers ℓ.

As written in (4), the kernel for the TA method is

$$D_{TA}(\mu,\tau) = (2\pi)^{-1}(2\pi\tau)^{-1/2}e^{-\zeta^2/2\tau}(d\zeta/d\mu). \tag{42}$$

The analysis of this kernel is similar to the analysis of the kernel for the Nanbu method presented in [6]. Conditions (38)-(40) are easily verified.

To verify (41), use $\mu = \cos\theta$ and $\zeta = \tan(\theta/2)$ to calculate for small τ

$$\begin{aligned}(2\pi/\tau)\int_{-1}^{1} d\mu D_{TA}(\mu,\tau)[1-P_\ell(\mu)] &= \tau^{-1}\int_0^\infty (2\pi\tau)^{-1/2} e^{-\zeta^2/2\tau}[1-P_\ell(\cos(2\arctan\zeta))]d\zeta \\ &= \tau^{-1}\int_0^\infty (2\pi)^{-1/2} e^{-\xi^2/2}[1-P_\ell(\cos(2\arctan\sqrt{\tau}\xi))]d\xi \\ &\approx \tau^{-1}(2\pi)^{-1/2}\int_0^\infty (2\pi)^{-1/2} e^{-\xi^2/2}\tau\xi^2\ell(\ell+1)d\xi \\ &\approx \ell(\ell+1). \end{aligned} \tag{43}$$

These calculations use the expansion $P_\ell(\cos(2\arctan\sqrt{\tau}\xi)) \approx 1 - 2\tau\xi^2 P'_\ell(1)$ for small τ and $P'_\ell(1) = \ell(\ell+1)$.

B Detailed Balance for Binary Collisions with Thermalization/Dethermalization

For collisions between particles of a single species, omit the subscripts α and β in (3) to obtain

$$f(\mathbf{v}) = \int_{R^3\times S^2} d\mathbf{w}d\mathbf{n}D(\frac{\mathbf{g}\cdot\mathbf{n}}{g}, \Lambda\frac{\Delta t}{g^3}) f(\mathbf{v}',t)f(\mathbf{w}',t). \tag{44}$$

Using the requirement [6] that $\int_{S^2} d\mathbf{n}D = 1$ equation (44) can be written as the following equation for the change Δf in time Δt

$$\Delta f(\mathbf{v}) = \int_{R^3\times S^2} d\mathbf{w}d\mathbf{n}D(\frac{\mathbf{g}\cdot\mathbf{n}}{g}, \Lambda\frac{\Delta t}{g^3}) \left\{ f(\mathbf{v}',t)f(\mathbf{w}',t) - f(\mathbf{v},t)f(\mathbf{w},t)\right\} \tag{45}$$

which will be used in the formulation of detailed balance conditions.

The equation (44) can be rewritten to include thermalization and dethermalization. Since it is an equation for $f(\mathbf{v})$, the thermalization/dethermalization is only applied to the terms $f(\mathbf{v})$ and $f(\mathbf{v}')$ inside the integral. Using the representation $f = m + k$, the integral on the right side of (3) becomes

$$\begin{aligned}\int_{R^3\times S^2} d\mathbf{w}d\mathbf{n}D \Big\{ \Big[m(\mathbf{v}')m(\mathbf{w}') + (1-p_D)m(\mathbf{v}')k(\mathbf{w}') + p_T k(\mathbf{v}')f(\mathbf{w}')\Big] \\ + \Big[p_D m(\mathbf{v}')k(\mathbf{w}') + (1-p_T)k(\mathbf{v}')f(\mathbf{w}')\Big]\Big\}. \end{aligned} \tag{46}$$

in which

$$D = D(\frac{\mathbf{g}\cdot\mathbf{n}}{g}, \Lambda\frac{\Delta t}{g^3}). \tag{47}$$

Note that dethermalization is not applied to the term $m(\mathbf{v}^{'})m(\mathbf{w}^{'})$. In the integral (46) and in all of the formulas below p_D and p_T are evaluated at $\mathbf{v}$, since the thermalization/dethermalization is applied after the collision. The terms in the first set of square brackets are the terms that contribute to the thermal component; while those in the second set of square brackets are the terms that contribute to the kinetic component. The contributions to the thermal component are projected onto a Maxwellian, so that

$$\begin{aligned} m(\mathbf{v}, t+\Delta t) &= \Pi_M \int_{R^3\times S^2} d\mathbf{w}d\mathbf{n}D\Big[m(\mathbf{v}^{'})m(\mathbf{w}^{'}) + (1-p_D)m(\mathbf{v}^{'})k(\mathbf{w}^{'}) \\ &\quad + p_T k(\mathbf{v}^{'})f(\mathbf{w}^{'})\Big] \qquad (48) \\ k(\mathbf{v}, t+\Delta t) &= \int_{R^3\times S^2} d\mathbf{w}d\mathbf{n}D\Big[p_D m(\mathbf{v}^{'})k(\mathbf{w}^{'}) + (1-p_T)k(\mathbf{v}^{'})f(\mathbf{w}^{'})\Big] \qquad (49) \end{aligned}$$

The projection in (48) is equivalent to the following equations for n_m, $\mathbf{u}_m$ and T_m

$$\begin{aligned} (n_m, n_m\mathbf{u}_m, n_m T_m)(t+\Delta t) &= \int_{R^3\times R^3\times S^2} d\mathbf{v}d\mathbf{w}d\mathbf{n}D\left(1, \mathbf{v}', |\mathbf{v}'-\mathbf{u}_m|^2/2\right) \qquad (50) \\ &\quad \Big[m(\mathbf{v}^{'})m(\mathbf{w}^{'}) + (1-p_D)m(\mathbf{v}^{'})k(\mathbf{w}^{'}) + p_T k(\mathbf{v}^{'})f(\mathbf{w}^{'})\Big]. \end{aligned}$$

As in equation (45), these can be rewritten as equations for the change in k and in n_m, $\mathbf{u}_m$ and T_m; i.e.,

$$\begin{aligned} &(\Delta n_m, \Delta(n_m\mathbf{u}_m),\ \Delta(n_m T_m)) \\ &= \int_{R^3\times R^3\times S^2} d\mathbf{v}d\mathbf{w}d\mathbf{n}D\Big\{\left(1, \mathbf{v}', |\mathbf{v}'-\mathbf{u}_m|^2/2\right)\Big[m(\mathbf{v}^{'})m(\mathbf{w}^{'}) + (1-p_D)m(\mathbf{v}^{'})k(\mathbf{w}^{'}) \\ &\quad + p_T k(\mathbf{v}^{'})f(\mathbf{w}^{'})\Big] - \left(1, \mathbf{v}, |\mathbf{v}-\mathbf{u}_m|^2/2\right)m(\mathbf{v})f(\mathbf{w})\Big\} \qquad (51) \end{aligned}$$

$$\Delta k(\mathbf{v}) = \int_{R^3\times S^2} d\mathbf{w}d\mathbf{n}D\Big\{p_D m(\mathbf{v}^{'})k(\mathbf{w}^{'}) + (1-p_T)k(\mathbf{v}^{'})f(\mathbf{w}^{'}) - k(\mathbf{v})f(\mathbf{w})\Big\}. \tag{52}$$

The detailed balance condition says that in equilibrium ($f = m+k = M$), each process and the reverse process exactly cancel. For equations (51) and

(52), this says that

$$
\begin{aligned}
0 &= \left(1, \mathbf{v}', |\mathbf{v}'|^2\right) \left[m(\mathbf{v}')m(\mathbf{w}') + (1-p_D)m(\mathbf{v}')k(\mathbf{w}') + p_T k(\mathbf{v}')f(\mathbf{w}')\right] \\
&- \left(1, \mathbf{v}, |\mathbf{v}|^2\right) m(\mathbf{v})f(\mathbf{w}) \qquad (53) \\
0 &= \left[p_D m(\mathbf{v}')k(\mathbf{w}') + (1-p_T)k(\mathbf{v}')f(\mathbf{w}')\right] - k(\mathbf{v})f(\mathbf{w}) \qquad (54)
\end{aligned}
$$

so that the thermalization and dethermalization conserve particle number, momentum, and kinetic energy. Although these conditions are not used in the hybrid method formulated above, they may be useful for improving the current hybrid method.